Research Article

Ding Chen*, Di Mu, Dachuan Chen, and Jinping Ni

Analysis on the speed properties of the shock wave in light curtain

https://doi.org/10.1515/phys-2022-0007
received October 31, 2021; accepted January 19, 2022

Abstract: In this study, we propose an improved measurement method based on light-curtain sensor, and it can obtain the hitting coordinates of supersonic projectile in a larger dispersion area. First, we analyze the speed properties of the shock wave in an effective detection area (also called light curtain in our field), and then find their change rules related to several key factors, including flight speed of the projectile, its attitude, shape, and the temperature in the testing environment. Next we improve a measurement system using wide-angle light-curtain sensor combined with calibration device of the shock speed; especially, this device with three parallel laser beams can effectively measure the shock speed in the light curtain. According to the related structural relation, we derive several computational formulas combined with the shock speed to obtain the hitting position of the measured projectile. Through live ammunition experiments, the results show that the proposed method is feasible and reliable for the supersonic projectile. Besides high accuracy, it also has many advantages, such as fewer sensors, lower requirement for installation, and larger detection area, by comparison with previous measurement systems.

Keywords: light-curtain sensor, supersonic projectile, hitting coordinates measurement, shock wave, calibration of the shock speed

*** Corresponding author: Ding Chen,** School of Armament Science & Technology, Xi'an Technological University, Xi'an 710021, China, e-mail: xatu@vip.qq.com
Di Mu: School of Armament Science & Technology, Xi'an Technological University, Xi'an 710021, China
Dachuan Chen: School of Aviation Basic, Aviation University Air Force, Changchun 130000, China
Jinping Ni: Shaanxi Province Key Laboratory of Photoelectric Measurement and Instrument Technology, Xi'an Technological University, Xi'an 710021, China

1 Introduction

For various barrel weapons (*i.e.*, pistol, rifle, machine gun, *etc.*), shooting accuracy is a key performance parameter. In the field, its concept can be usually described as a statistic of deviation from all hitting coordinates to the center of their dispersion. Accordingly, people always expect the hitting coordinates of every projectile to be accurately measured. Nowadays, more advanced weapons (*e.g.*, electromagnetic gun, missile with scram-jet engine, *etc.*) have longer effective shooting range (*i.e.*, 1,000 m and longer); generally, the projectile speed is beyond five times that of sound. Moreover, this also brings about a large dispersion radius of their projectile holes on the target due to some interference factors, such as jump angle, wind speed, wind direction, air density, air temperature. Obviously, this requires a larger detection area (up to 10 m $\times$ 10 m), and high measurement accuracy and reliability. For the supersonic projectile, the measurement of its hitting coordinates thus face more serious challenges due to the above high requirements.

In the past few decades, some measurement methods have been proposed for using in this application. Generally, bullet holes on the wooden (or steel) target plate can be directly measured by high-resolution digital camera [1]. Through image recognition [2], its measurement accuracy can be even up to the pixel level. Unfortunately, some overlapping bullet holes are probably neglected. In addition, the larger the target plate is, the higher the wind drag is. Consequently, this needs more and stronger structural supports. They are usually disposable so this causes a great deal of waste of wood or steel. A photoelectric testing system with intersecting detection areas has several invisible target plates (also called light curtain) [3]. In essence, it forms an effective detection area using some components (*i.e.*, LED array or infrared diode array, light-curtain sensors, photoelectric signal processing module, *etc.*). Thus, there is no consumption of wood or steel at all. Especially, it cannot only measure the hitting coordinate of the projectile but also its flying velocity, attitude angle, *etc.*; in addition, this method has almost no limit of the projectile velocity.

Unfortunately, its detection area is hard to expand beyond 5 m × 5 m. Besides, a measurement system based on triangular light-curtain sensor combined with intersecting-charge coupled device vertical targets has measurement precision of millimeter-level [4], and yet there is also a similar problem, that is, its detection area is below 5 m × 5 m. Moreover, a measurement system based on laser forms a line laser screen with inverted triangular shape [5]. If a projectile passes through the laser screen, several laser detection sensors can detect its echo signal [6]. On the basis of the temporal and spatial domain detection model [7], the hitting coordinates of the projectile can be obtained. In the system, the laser power is uniformly spread on the line laser screen. To ensure the detection performance for a higher flying projectile, a higher power laser should be used. As a result, this brings about higher cost, increased weight, difficulty in maintenance, *etc.* According to acoustic characteristic of the shock wave [8], an acoustic sensor-based measurement system and its improved system can also measure the hitting coordinates of supersonic projectile. After a supersonic projectile perpendicularly passes through the detection area, several acoustic sensors can detect the sound pressure from the measured projectile [9]. Due to the difference in arrival time of their acoustic waves, the coordinates of the measured projectile can be calculated by a calculation model [10]. However, it needs more acoustic sensors if the detection area is larger,10 m × 10 m. Unfortunately, this probably brings about a series of problems, such as complex structure, high cost, inconvenience to maintain, and poor reliability. In previous study, we developed a measurement system with the larger light curtain of 10 m × 10 m through multi-lens splicing [11, 12]. However, this system can only measure the flying velocity of the supersonic projectile using two parallel light curtains. In this study, we want to further improve the previous measurement systems and focus mainly on how to effectively measure the hitting coordinates of the supersonic projectile. Moreover, it should also have major advantages of large detection area, high accuracy, and high reliability. Considering the advantages of the other methods, it will be a better choice that the proposed method based on light-curtain can be combined with different methods.

Therefore, we propose an improved measurement method based on light-curtain sensor considering the shock wave effect to obtain the hitting coordinates of a supersonic projectile. First, we describe briefly forming mechanisms of the shock wave caused by the supersonic projectile. Furthermore, we analyze some changing trends of the shock speed affected by several factors (*i.e.*, flight speed of the projectile, shape of the projectile head, and the temperature in the testing environment). Next we mainly use a light-curtain detector and L-shaped LED array to form a rectangle light curtain, which has three sub-detection areas. Besides, we bring forward an effective approach for acquiring the actual shock speed in the light curtain using a calibration device with three parallel lasers. Then, we investigate three calculation models of the hitting coordinates in three different sub-detection areas, respectively. Finally, the feasibility and effectiveness of the proposed method can be verified through live ammunition experiments.

2 Analysis of shock speed in the light curtain

2.1 Formation principle of the shock wave caused by supersonic projectile

Before the study, it is important to note that the mentioned projectiles in the study are all without tail wing, and their head shape can be approximated to a cone. After a supersonic projectile passes through the light curtain, the light-curtain sensor outputs two signals, as shown in Figure 1. Through high-speed photography [13], we can obtain the time when the projectile arrives on the light curtain. Accordingly, the left signal should be generated by the projectile. Through many observations in the measurement, it is found that the time interval between the two signals is proportional to the distance between the sensor and the penetration position in the light curtain.

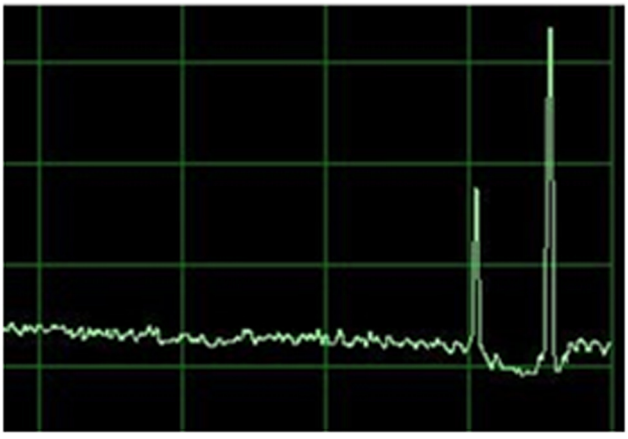

Figure 1: Two output signals on an oscilloscope after a supersonic projectile passes through the light curtain.

After analysis, it is found that the other signal is caused by an acoustics phenomenon called shock wave effect. When a projectile flies with supersonic speed and cone shape head, the air in its front can be compressed and split to form a high-density air layer with cone-like shape (Figure 2). The above physical processes, and the forming principle of the shock wave is described in brief in ref. [8]. Similar to acoustic wave, the shock wave is also a disturbance wave in nature. However, its speed properties are different from that of the acoustic wave. For the supersonic projectile, it leads to an oblique shock wave because its shock front is not perpendicular to the airflow direction; herein the high-density air layer is also called shock front, and the airflow direction is inverse to that of the flight projectile. Therefore, there is an angle between the shock front and the airflow direction defined as the Mach angle which is usually expressed by ref. [8]

$$\alpha = \arcsin\left(\frac{c}{v}\right) = \arcsin\left(\frac{1}{\mathrm{Ma}}\right), \tag{1}$$

with

$$c = c_0 \cdot \sqrt{1 + t_\mathrm{L}/T_0}, \tag{2}$$

where α is the Mach angle, v is the flying speed of the supersonic projectile, c is the acoustic speed in the testing environment, Ma is the Mach number, c_0 is the acoustic speed when the temperature is 0°C, t_L is the Celsius temperature in the light curtain, and T_o is the thermodynamic temperature corresponding to the Celsius temperature of 0°C. In this study, we suppose that c_0 and T_o are 331.45 m s^{-1} and 273.15 K, respectively.

During the flight of the supersonic projectile, a series of disturbance waves constantly appear on the rear of the supersonic projectile, and they diffuse outwards in the form of the spherical wave. In Figure 2, only a circle is drawn for convenience. Obviously, the shock speed can be decomposed into two different vectors. One of them is orthogonal to the shock front, and the shock speed at the direction is always equal to the acoustic speed in the testing environment. Obviously, this can enlighten us on the idea of how to solve the current problem.

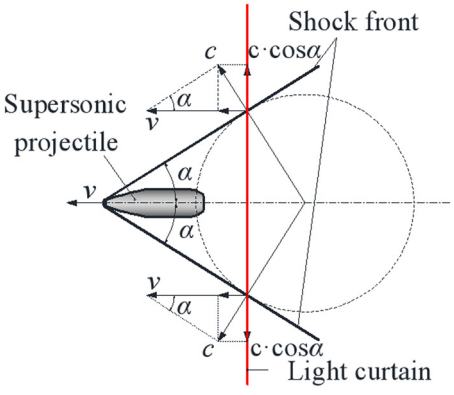

Figure 2: Analytical diagram of the speed property of the shock wave if the projectile flight speed is lower than the critical value.

2.2 Changing trends of shock speed in the light curtain determined by key factors

2.2.1 Models of shock speed in the light curtain

Before analysis, we made a series of assumptions as following. The air is stationary and it has the constant heat ratio; especially, the airflow viscosity and thermal conductivity can be neglected. Besides, the measured projectile without tail wing is approximated to a combination of cone and cylinder, and its surface is also smooth. Ideally, the supersonic projectile perpendicularly passes the light curtain.

Therefore, a part of the shock wave in the light curtain spreads out at the center of the projectile's penetration position. In fact, it is not the acoustic speed but a projection of that on the light curtain, and it is given by

$$c_\mathrm{L} = c \cdot \cos\alpha = c \cdot \sqrt{1 - (c/v)^2}, \tag{3}$$

where c_L is the shock speed in the light curtain.

According to equation (1), the Mach angle decreases with the increment in the projectile speed. In other words, the conical degree of the high-density air layer also decreases with the increment in the projectile speed.

After the projectile speed increases to a critical value, the Mach angle cannot decrease even if the flight speed increases further. This is because the shock front is limited by the projectile head shape, as shown in Figure 3. Under this condition, the shock wave relatively remains stable. The critical value of the projectile speed is given by

$$v_\mathrm{c} = c/\sin\mu, \tag{4}$$

where μ is the half-conical angle of the projectile head.

Moreover, the shock speed in the light curtain is also given by

$$c_\mathrm{L} = c \cdot \cos\mu. \tag{5}$$

For a certain projectile, this shock speed in the light curtain is mainly affected by some key factors, which are the flight speed, head shape of the projectile, and the temperature in the light curtain.

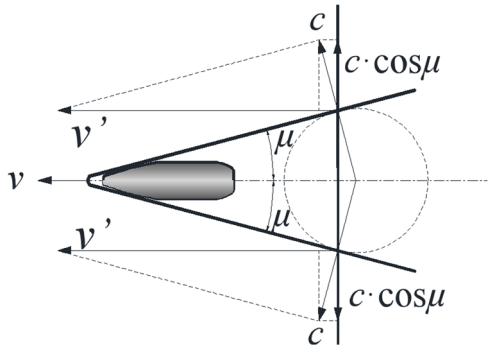

Figure 3: Analytical diagram of the speed property of the shock wave if the projectile flight speed is higher than the critical value.

2.2.2 Effects of several key factors

Suppose that the half-conical angle of the projectile head is a certain value (*i.e.*, 15°), then we consider the effects of only two factors, which are the projectile speed and the temperature in the testing environment. Variable range of the former is from 150 to 2,150 m s^{-1}, and that of the latter is from −40 to 60°C. Based on equations (1)–(5), we can observe the changing trends of the shock speed in the light curtain dominated by the above two factors, as shown in Figure 4.

On the one hand, the shock speed in the light curtain increases with the increment in the temperature in the testing environment, and this obeys the physical laws between the acoustic speed and the temperature. On the other hand, the shock speed dramatically increases with the increment of the projectile speed, and yet it begins to slowly increase if the Mach angle is gradually coming close to the conical angle of the projectile head. Finally, it remains basically unchanged. In addition, Figure 4 shows that there is no shock speed in the light curtain if the projectile speed is below the acoustic speed.

In the next analysis, we assume that the temperature in the testing environment is 25°C. In addition, the conical angle and speed of the measured projectile are variable from 0° to 180° and from 150 to 2,150 m s^{-1}, respectively. We analyze the effects of the projectile speed and its head shape. Based on equations (1)–(5), we find the changing trends of the shock speed in the light curtain dominated by these two factors as shown in Figure 5. For the projectile speed, the changing trend of the shock speed in the light curtain is also in accordance with the previous analysis. However, we find that the shock speed in the light curtain increases with the decrease in the conical angle of the projectile head. If the conical angle is 180°, the projectile will become a plane. This leads to the normal shock wave so that the component of the shock wave cannot propagate in the light curtain. If the conical angle of the projectile head is close to 0°, it is approximately deemed to be a straight line. In this case, the shock speed in the light curtain is nearly the acoustic speed.

In the measurement of shooting accuracy, the projectile is desired to perpendicularly pass through the target plate, and this also means that its predicted ballistic trajectory should be perpendicular to the light curtain. Unfortunately, there are generally some deviations between the predicted and actual ballistic trajectory due to some interference factors. To simplify the analysis, we suppose that there is only the pitch angle of the projectile but without the azimuth angle in the following analysis.

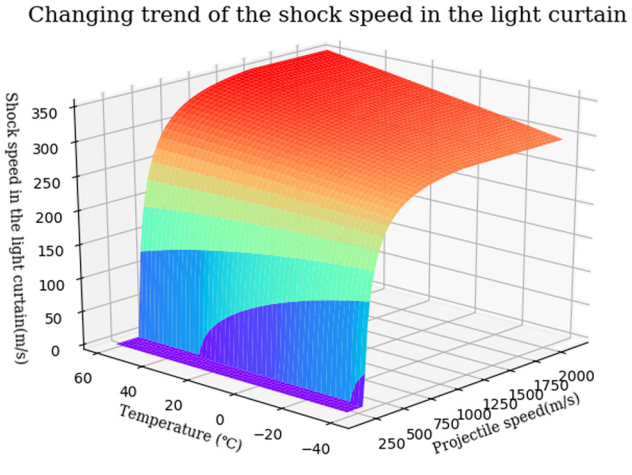

Figure 4: Changing trend of the shock speed in the light curtain affected by the projectile speed and the temperature in the testing environment.

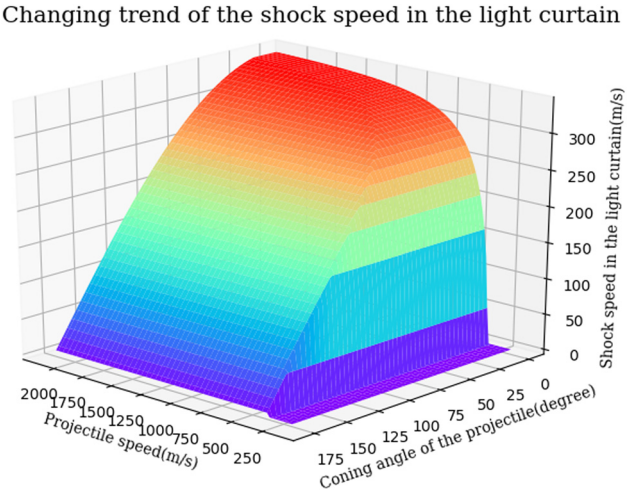

Figure 5: Changing trend of the shock speed in the light curtain affected by the projectile speed and its head shape.

Through related geometric transformations, we can obtain two shock speeds with two different directions in the light curtain (Figure 6), and their expressions can be given by

$$c_{\mathrm{d}} = \begin{cases} c \cdot \cos(\theta - \alpha), & \text{if} \quad \alpha > \mu, \\ c \cdot \cos(\theta - \mu), & \text{if} \quad \alpha \le \mu, \end{cases} \tag{6}$$

and

$$c_{\mathrm{u}} = \begin{cases} c \cdot \cos(\theta + \alpha), & \text{if} \quad \alpha > \mu, \\ c \cdot \cos(\theta + \mu), & \text{if} \quad \alpha \le \mu, \end{cases} \tag{7}$$

where c_{u} and c_{d} are the two shock speeds in the light curtain, c is the acoustic speed in the testing environment, α is the Mach angle, μ is the half-conical angle of the projectile head, and θ is the pitch angle of the projectile.

Again, we make a series of assumptions as follows. For the measured projectile, its half-conical angle is 15° and the temperature in the testing environment is 25°C. Specially, the range of its pitch angle is from –5° to 5° and that of the projectile speed is from 150 to 2,150 m s^{-1}.

According to equations (4) and (7), we can obtain the maximum relative error of the shock speed caused by the pitch angle, and its expression is given by

$$\delta_{\mathrm{Max}} = \mathrm{Max}\left(\left| \frac{c_{\mathrm{L}} - c_{\mathrm{u}}}{c_{\mathrm{L}}} \right|, \left| \frac{c_{\mathrm{L}} - c_{\mathrm{d}}}{c_{\mathrm{L}}} \right| \right) \times 100\%, \tag{8}$$

where c_{L} is the shock speed in the light curtain if the projectile is without the attitude angle, that is, its trajectory is perpendicular to the light curtain.

In Figure 7, it is shown that the greater the pitch angle is, the larger the maximum relative error of the shock speed is. Only if the pitch angle is zero, the error of the shock speed in the light curtain will vanish. Besides, we also find that the higher speed of the projectile can contribute to decrease in the error of the shock speed in the light curtain.

Furthermore, we also want to take into consideration the effect of temperature. Assuming that the range of its pitch angle is from –5° to 5°, and the half-conical angle of the projectile head is 15°, but the projectile speed is constant at 1,750 m s^{-1}, the range of the temperature in the testing environment is from –40 to 60°C. Figure 8 shows that the error of the shock speed in the light curtain is in proportion to the pitch angle. Similarly, pitch angle of 0° is corresponding to non-existence of the error. In addition, the temperature cannot have any influence on the error of the shock speed in the light curtain. In fact, the measured projectile has not only the attitude angle but also the azimuth angle. In the light curtain, inconsistency of the shock speed in different directions will become more serious under this condition. Ideally, the cone of the shock front is circular in the crossing section on the light curtain if the ballistic trajectory of the measured projectile is perpendicular to the light curtain. The shock in the light curtain spreads out at the center of a circle, and the shock speed in each direction is uniform. In fact, it is not impossible that the ballistic trajectory is not absolutely perpendicular to the light curtain. As a result, this leads the cone of the shock front to become elliptical in crossing section on the light curtain. In the light curtain, the shock speed in each direction is not obviously uniform. According to the above analysis, the difference among the shock speed in different directions is bound up with an inclination of the ballistic trajectory.

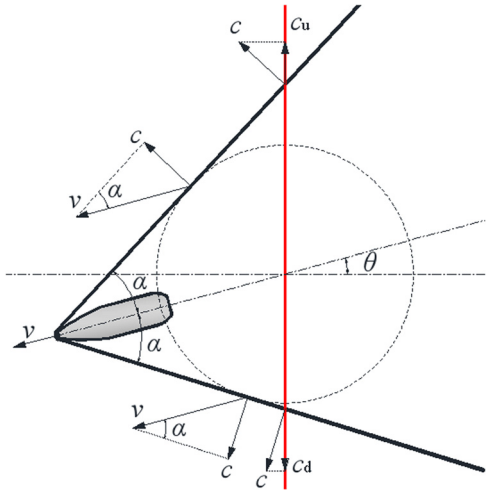

Figure 6: Analytical diagram of the speed property of the shock wave if the ballistic trajectory is not perpendicular to the light curtain.

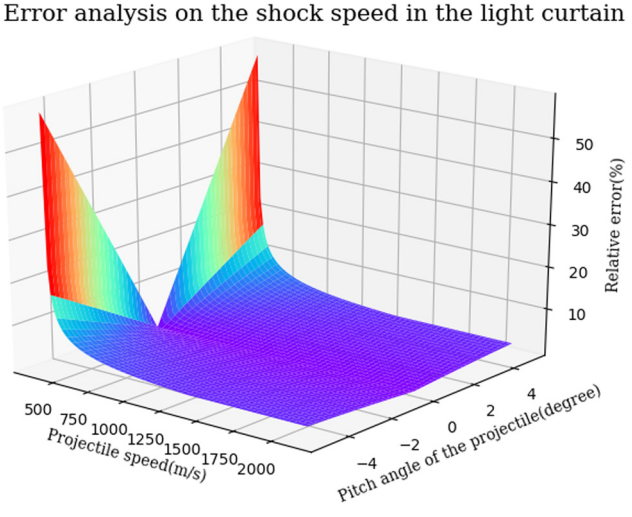

Figure 7: Changing trend of the relative error of the shock speed in the light curtain affected by the projectile speed and the attitude angle of the projectile.

Currently, all advanced barrel weapons have direct aiming device so that the jump angle of their barrel is generally very small and below 1′.

This means that their ballistic trajectory can be deemed to be a straight line in the effective shooting range. To improve the aerodynamics performance, the shape of their projectile head is designed to be very sharp, that is, the half-conical angle is not very large. Crucially, they have higher flight speed beyond five times that of sound. Obviously, these excellent characteristics can effectively reduce the inconsistency of the shock speed in the light curtain caused by the attitude angle of the projectile.

In theory, if the shock speed in the light curtain can be accurately calculated, we use several sensors to correspondingly obtain several time-of-arrival (TOA) parameters of the projectile's shock wave. Further, location information of this projectile should also be obtained according to structural relation between these sensors. As mentioned above, the shock speed is affected by many factors. Unfortunately, some factors, especially the projectile speed and temperature, are usually variable, random, and unpredictable. This also brings about time-varying shock speed in the light curtain. Consequently, the shock speed in the light curtain cannot be accurately calculated through the formulas proposed in this section. Their function is only to help us to better discover some main changing trend of shock speed in the light curtain. Even in the light curtain with 10 m × 10 m, the spread time of the shock wave also has only dozens of milliseconds. In the very short time, the shock speed is considered to be constant. Therefore, we should develop a calibration device to effectively obtain the real-time shock speed in the light curtain.

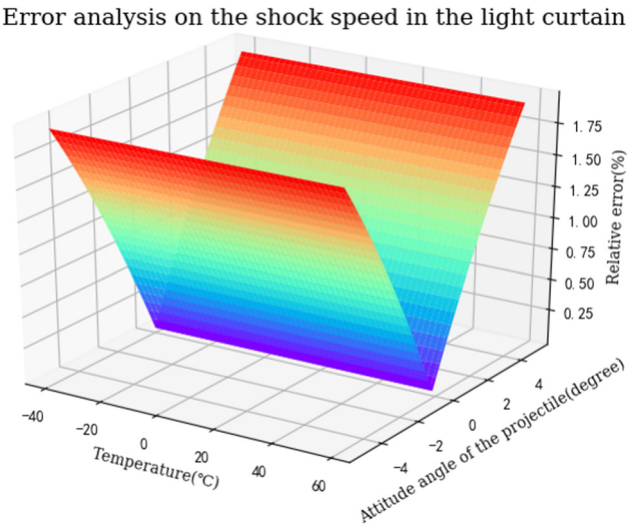

Figure 8: Changing trend of the relative error of the shock speed in the light curtain affected by the attitude angle of the projectile and temperature in the testing environment.

3 Measurement method

The proposed measurement system (Figure 9) is chiefly composed of main measurement device, calibration device of the shock speed, data acquisition module, signal and data processing module, display and control module, and so on. In the system, there are two key components, and they are the main measurement device and the calibration device of the shock speed.

3.1 Main measurement device

The main measurement device mainly consists of a light curtain sensor and two LED arrays, as shown in Figure 10.

Specially, the light curtain sensor has three similar lenses which can form a fan-shaped detection area with the viewing angle of 30° and less thickness (usually, less than 1 mm). Thus, they can be structured to a detection area with the viewing angle of 90° by adopting multi-lens splicing technology [11]. Most importantly, three detection areas must be co-planar through adjustments. In fact, this detection area is separated into three parts (*i.e.*, three sub-detection areas), which are detection areas I, II, and III. Besides, we must use optical filters to avoid interference of light with certain wavelengths.

In fact, the light curtain sensor is a passive photoelectric detection system. Thus, we must provide some artificial light sources (*i.e.*, LED array) for it, and this can form a bright background with reasonable light distribution. Consequently, the light in the detection area can be received by the three lenses of the light curtain

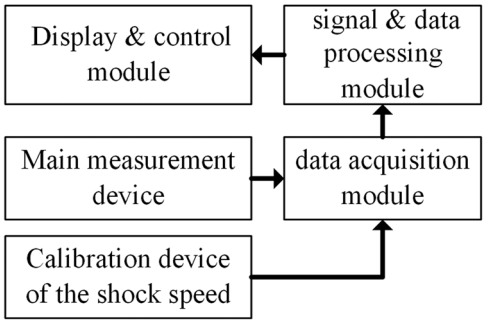

Figure 9: Block schematic of the measurement system.

sensor. When a flying target passes through the light curtain, the light received by the lens decreases steeply. When a flying projectile with supersonic speed passes through a sub-detection area in the light curtain, three measurement channels in the data acquisition module correspondingly generate several signals, which are a pulse signal of the flying projectile and three pulse signals of the shock wave. The time interval values among these signals are accurately obtained through related estimation methods [14–16], and thus we can measure the distance from the penetration position to the lens and the two minimum those from this penetration position to other two sub-detection areas, respectively. However, this must meet some requirements as follows. First, key structural parameters of the three sub-detection areas and other components are all known and calibrated in advance. This problem has been solved in our previous work [17]. Besides, real-time shock speed in the light curtain should also be known. Obviously, this problem is crucial to our study. In Section 3.2, a calibration device is developed to effectively obtain the shock speed in the light curtain.

3.2 Calibration device for the shock speed

In Figure 10, there are three pairs of laser transmitters and receivers, and their function is to calibrate the shock speed in the light curtain. To highlight the three pairs of laser transmitters and receivers, they are plotted in Figure 11. Through installations and adjustments, these three transmitters can emit three parallel laser beams; correspondingly, those three receivers must accurately receive them. Especially, these parallel laser beams should be in the light curtain, and the distance between any two adjacent laser beams must also be equal. Most importantly, their wavelength should be different so that each receiver cannot be jammed by other lasers. In fact, optical filters in the main measurement device are to prevent these three lasers from interfering its detection effect. Moreover, these lasers also have high enough power and continuous emission.

In theory, transmission characteristic of the laser is also affected by the shock wave from a supersonic projectile in the light curtain. Subsequently, every receiver can detect the change in its corresponding laser. Like the light curtain sensor, the change in the laser beams can also be translated into signals through related processing. Next we use wavelet transform modulus maximum method [18,19] to extract time when the shock wave arrives at the three laser beams. Due to the known distance between these parallel laser beams, we can calculate the shock speed in the light curtain.

We can observe that these three laser beams divide the light curtain into four areas (*i.e.*, areas A, B, C, and D). Assuming that the distance between any two adjacent laser beams is S and t_P is the time when the measured projectile passes through the light curtain, and in addition, t_1, t_2, and t_3 are the time when the shock wave arrives at the three laser beams, then we can obtain three expressions given by

$$c_1 = \frac{2S}{|t_1 - t_3|}, \tag{9}$$

$$c_2 = \frac{S}{|t_1 - t_2|}, \tag{10}$$

and

$$c_3 = \frac{S}{|t_2 - t_3|}, \tag{11}$$

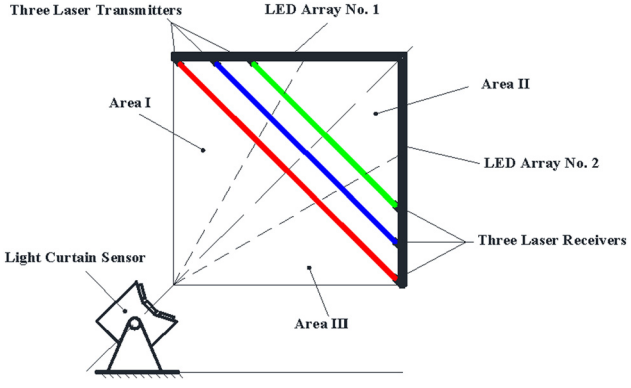

Figure 10: Schematic diagram of the main measurement device.

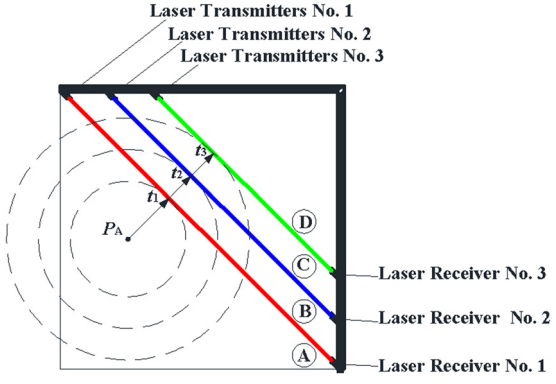

Figure 11: Schematic diagram of the calibration for the shock speed in the light curtain if the penetration position of the supersonic projectile is at the area A.

For better accuracy, final calculation expression is given by

$$c = \frac{\frac{2S}{|t_1 - t_3|} + \frac{S}{|t_1 - t_2|} + \frac{S}{|t_2 - t_3|}}{3}. \tag{12}$$

Likewise, the shock speed can also be calculated using equation (12) if the penetration position is in the area *D*.

Next if the penetration position is in the area *B* or *C*, an integrated calculation expression of the shock speed is given by:

$$c = \frac{\frac{2S}{|t_1 + t_3 - 2t_P|} + M_1 + M_2}{3}, \tag{13}$$

with

$$M_1 = \frac{S}{|t_2 - \mathrm{Max}(t_1, t_3)|}, \tag{14}$$

and

$$M_2 = \frac{S}{|\mathrm{Min}(t_1, t_3) + t_2 - 2t_P|}. \tag{15}$$

In engineering, there are some small probability events, that is, the penetration position is just in a laser beam. In fact, this has little influence on the above calibrations. Because the shock speed in the light curtain is known after calibrations, we can effectively obtain the hitting coordinates of the measured projectile through some calculation models, and they will be discussed below in more detail in Section 3.3.

3.3 Calculation models

We establish a rectangular coordinate system, and its original point is O, which is the common focus of the three lenses (Figure 12). Ideally, the field angles of α_I, α_{II}, and α_{III} are all 30°. The boundary between the areas I and II is O–M, and that of the areas II and III is O–N.

As seen in Figure 12, a supersonic projectile passes through the area I in the light curtain, and its penetration position is called P. First, the shock front arrives at a point, which is defined as D_M, in the boundary between the areas I and II. Next the shock front arrives at another point, which is defined as D_N, in the boundary between the areas II and III. Finally, the shock front arrives at the point of O. Through, wavelet transform modulus

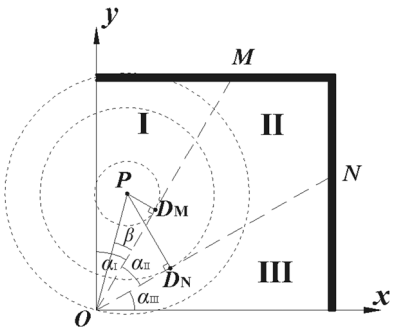

Figure 12: Schematic diagram of the calculation model under the condition that the penetration position is in the area I.

maximum method [18,19], we can obtain three TOA parameters (*i.e.*, t_P, t_M, and t_N) corresponding to the three points of P, D_M, and D_N.

In a right triangle of ΔPOD_M, an angle of $\angle POD_M$ is defined as β, and the distance between P and D_M is defined as PD_M, which can be obtained by

$$PD_M = PO \cdot \sin\beta = |t_P - t_M| \cdot c, \tag{16}$$

where PO is the distance between P and O and c is the shock speed in the light curtain.

Through observation, an angle of $\angle POD_N$ should be

$$\angle POD_N = \beta + \alpha_I. \tag{17}$$

In a right triangle of ΔPOD_N, PD_N is the distance between P and D_N and can be obtained by

$$PD_N = PO \cdot \sin\angle POD_N = |t_P - t_N| \cdot c. \tag{18}$$

Substituting equation (17) in equation (18) can produce

$$PD_N = PO \cdot \sin(\beta + \alpha_I) = |t_P - t_N| \cdot c. \tag{19}$$

According to equations (16) and (19), we can give a proportional relation between them, and it is expressed by

$$\frac{PD_N}{PD_M} = \frac{\sin(\beta + \alpha_I)}{\sin\beta} = \sin\alpha_I \cdot \cot\beta + \cos\alpha_I = \frac{|t_P - t_N|}{|t_P - t_M|}. \tag{20}$$

Next $\cot\beta$ in equation (20) can be directly solved, and its expression is

$$\cot\beta = \frac{\frac{|t_P - t_N|}{|t_P - t_M|} - \cos\alpha_I}{\sin\alpha_I}. \tag{21}$$

Through transformation of the inverse trigonometric function, we can thus obtain the angle of β, which is given by

$$\beta = \cot^{-1}\left(\frac{|t_P - t_N|}{|t_P - t_M| \cdot \sin\alpha_I} - \cot\alpha_I\right). \tag{22}$$

Finally, we can obtain the calculation model of the P penetration position based on 2–dimensional (2D) coordinates and they are

$$\begin{aligned} x &= PO \cdot \cos(\alpha_I - \beta) \\ &= \frac{|t_P - t_M| \cdot c}{\sin\beta} \cdot \cos(\alpha_I - \beta), \end{aligned} \tag{23}$$

and

$$\begin{aligned} y &= PO \cdot \sin(\alpha_I - \beta) \\ &= \frac{|t_P - t_M| \cdot c}{\sin\beta} \cdot \sin(\alpha_I - \beta). \end{aligned} \tag{24}$$

Likewise, for the other two cases, we can also give their calculation models.

If the penetration position is in the area II, its calculation formula can be expressed by

$$\begin{aligned} x &= PO \cdot \cos(\alpha_{III} + \gamma) \\ &= \frac{|t_P - t_N| \cdot c}{\sin\gamma} \cdot \cos(\alpha_{III} + \gamma), \end{aligned} \tag{25}$$

with

$$\gamma = \cot^{-1}\left(\frac{|t_P - t_M|}{|t_P - t_N| \cdot \sin\alpha_{II}} + \cot\alpha_{II}\right), \tag{26}$$

and

$$\begin{aligned} y &= PO \cdot \sin(\alpha_{III} + \gamma) \\ &= \frac{|t_P - t_N| \cdot c}{\sin\gamma} \cdot \sin(\alpha_{III} + \gamma). \end{aligned} \tag{27}$$

If the penetration position is in the area III, its calculation formula can be expressed by

$$x = \frac{|t_P - t_N| \cdot c}{\sin\theta} \cdot \cos(\alpha_{III} - \theta), \tag{28}$$

with

$$\theta = \cot^{-1}\left(\frac{|t_P - t_N|}{|t_P - t_N| \cdot \sin\alpha_{III}} - \cot\alpha_{III}\right), \tag{29}$$

and

$$y = \frac{|t_P - t_N| \cdot c}{\sin\theta} \cdot \sin(\alpha_{III} - \theta). \tag{30}$$

Due to randomness of the penetration position, it may be on the boundary between any two areas, and then the shock front arrives on the other boundary. Under the condition, its calculation model will become simpler because of considering only one right triangle in area II. Accordingly, their calculation models can be given as follows.

$$x = \frac{|t_P - t_N| \cdot c}{\sin\alpha_{II}} \cdot \sin\alpha_I, \tag{31}$$

and

$$y = \frac{|t_P - t_N| \cdot c}{\sin\alpha_{II}} \cdot \cos\alpha_I, \tag{32}$$

if the penetration position is on the boundary of O–M.

Besides,

$$x = \frac{|t_P - t_M| \cdot c}{\sin\alpha_{II}} \cdot \sin\alpha_{III}, \tag{33}$$

and

$$y = \frac{|t_P - t_M| \cdot c}{\sin\alpha_{II}} \cdot \cos\alpha_{III}, \tag{34}$$

if the penetration position is on the boundary of O–N.

According to some time sequence differences among output signals of the data acquisition module, an appropriate calculation model can thus be determined to obtain the hitting coordinates of the measured flying projectile. In engineering, the calibration of the shock speed in the light curtain and calculation of the hitting coordinates should be immediately performed in the signal and data processing module. Finally, the calculation results are presented on the display and control module. Therefore, the proposed measurement system has the characteristic of higher real-time, reliability and accuracy.

4 Experiments and discussion

To test the validity of the improved measurement system based on light-curtain sensor, three measurement systems, including a wooden target and a measurement system based on acoustic sensor arrays and the proposed system, are established in an indoor shooting gallery with the cross-section of 10 m × 10 m. According to related technical standards [20], live ammunition experiments cannot be permitted under the terrible weather conditions. Thanks to the indoor shooting gallery, it can maintain a relatively stable environmental conditions, such as temperature (*i.e.*, 20 ± 2°C), humidity (*i.e.*, 65 ± 5%), and atmosphere.

Figure 13 shows a sectional view of the experimental setup in the indoor shooting gallery. It can be observed that a wooden target is installed on the vertical wall at the end of the indoor shooting gallery. Especially, the wooden target, the detection area of the acoustic sensor

arrays, and the light curtain should be in parallel, and their interval distances are all 1 m. Besides, a launch device based on electromagnetism is aimed at the center of the wooden target, and its presupposition ballistic trajectory, which is at a height of 5 m from the ground, must also be perpendicular to the wooden target. The distance from the gunpoint to the wooden target is approximately 500 m, and this distance is also within the effective firing range. Ideally, the flying trajectory of the projectile can thus be considered to be a straight line. Through digital image processing, we can measure the coordinate values of bullet holes on the wooden target, and the measurement error is not beyond 1 mm.

Assuming that the measurement results from the wooden target is the reference value or truth-value, we can also obtain two other sets of measurement results, which are from the improved system based on light-curtain sensor and acoustic sensor arrays. Generally, the measurement error of the acoustic system is less than 5 mm. For the launch device, the flying speed of its projectile is supersonic in its effective shooting range (generally, beyond 2,000 m). In addition, the projectile is fired through electronic control, and thus this can avoid some effects from hand operation. Therefore, for experimental results, we mainly take two factors into consideration, and they are the projectile speed and the projectile head shape.

4.1 Different speeds of the flying projectiles

In the first set of experiments, we use some projectiles with the same caliber and head shape (*i.e.*, the conical angle of 40 degrees). Through accurately adjusting current, 4 different speeds of the projectiles can be obtained, and they are respectively 1.5, 2, 3, and 5 times as large as that of sound in the indoor shooting gallery at the temperature of 20 ± 2°C. Under every condition of the projectile speed, we fire 100 projectiles and then record their coordinate values by adopting the three measurement systems (*i.e.*, wooden target based on image processing, sound microphone array, and the improved system based on light-curtain sensor), as shown in Figure 14.

We can observe that the dispersion radius of bullet holes cannot be larger than 5 m. Accordingly, the maximum jump angle of the weapon under test can be calculated, and it is 0.49°. According to the changing trend of the relative error of the shock speed in Section 2, the maximum relative error of the shock speed is only 0.15% if the attitude angle is 0.49°. Thus, this influencing factor can also be negligible.

Compared with the reference value, a set of measurement error data of the sound microphone array and the improved system based on light-curtain sensor can be obtained if the projectile speed is five times the speed of sound, as shown in Figure 14. Note that the dotted lines represent mean value, or they can also be seen as systematic error. Generally, the systematic error is mainly caused by structural assembly and electrical characters. However, the systematic error can be effectively compensated using some method [21]. Therefore, we adopt the standard deviation between measured data and ideal data to evaluate the measurement performance. In Tables 1–4, key performance judgments (*i.e.*, mean value, standard deviation, and maximum deviation) of the two systems are listed and compared under different

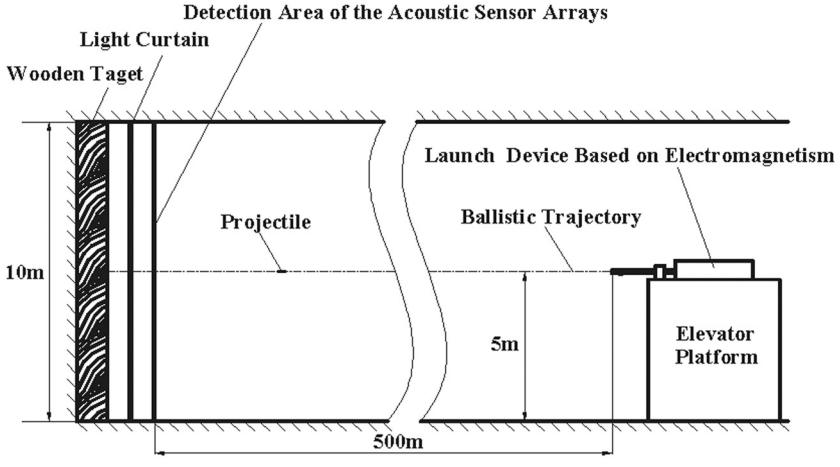

Figure 13: Sectional view of the experiment setup in the indoor shooting gallery.

Table 1: Key performance judgments of the two measurement systems under the condition of projectile speed 5 times that of sound

Type	Coordinates	Mean value (mm)	Standard deviation (mm)	Maximum deviation (mm)
Sound microphone array	x	0.6411	0.6411	2.5132
	y	−0.8339	0.3839	1.9999
Light-curtain sensor	x	0.5803	0.6001	1.9299
	y	−0.2268	0.8644	2.5005

Table 2: Key performance judgments of the two measurement systems under the condition of projectile speed 3 times that of sound

Type	Coordinates	Mean value (mm)	Standard deviation (mm)	Maximum deviation (mm)
Sound microphone array	x	0.8524	1.0596	2.8754
	y	0.8450	1.4522	4.275
Light-curtain sensor	x	0.9065	1.1555	3.8530
	y	1.0861	1.4021	4.4657

Table 3: Key performance judgments of the two measurement systems under the condition of projectile speed 2 times that of sound

Type	Coordinates	Mean value (mm)	Standard deviation (mm)	Maximum deviation (mm)
Sound microphone array	x	0.8040	3.3118	8.8581
	y	0.9587	2.9563	8.4903
Light-curtain sensor	x	0.2044	3.4425	7.9602
	y	1.1454	2.8533	9.0676

Table 4: Key performance judgments of the two measurement systems under the condition of projectile speed 1.5 times that of sound

Type	Coordinates	Mean value (mm)	Standard deviation (mm)	Maximum deviation (mm)
Sound microphone array	x	1.3832	3.9723	12.8651
	y	2.6196	5.1043	16.4207
Light-curtain sensor	x	1.9007	4.6260	12.2584
	y	1.1884	3.0373	8.9684

conditions of projectile speed, that is, 5, 3, 2, and 1.5 times the speed of sound.

From the above tables, we can conclude that with the increase in projectile speed, both the systems have better measurement results. Specifically speaking, their standard deviations also became smaller. However, we find that their measurement performance is no longer significantly improved even if the speed of the projectile is higher. On the contrary, when the projectile speed is slightly higher than that of sound, the measurement error is larger. Especially, when the projectile speed is very close to the sound speed, both these systems lost many measurement results. Obviously, these results are basically in line with the law that is analyzed and discussed in Section 2. Therefore, the two systems are better applied in the measurement of the hitting coordinates of some hypersonic targets.

4.2 Different shapes of the projectile head

In the second set of experiments, we used projectiles with the same caliber, but with different head shapes (*i.e.*, the conical angle). Their conical angles are 45°, 90°, and 120°. In addition, we properly adjusted the current of the launch device in such a way that the flying speed of the measured projectile can be up to three times that of sound in the effective shooting range. Moreover, the

Table 5: Key performance judgments of the two measurement systems under the condition of the conical angle of 90°

Type	Coordinates	Mean value/(mm)	Standard deviation/(mm)	Maximum deviation/(mm)
Sound microphone array	*X*	0.2507	1.1530	2.8498
	Y	0.4190	1.3890	3.9010
Light-curtain sensor	*X*	0.9768	1.2369	3.9066
	Y	1.1991	1.5210	3.8213

Table 6: Key performance judgments of the two measurement systems under the condition of the conical angle of 120°

Type	Coordinates	Mean value/(mm)	Standard deviation/(mm)	Maximum deviation/(mm)
Sound microphone array	*X*	0.5589	1.2421	3.5856
	Y	0.7612	1.5991	4.8640
Light-curtain sensor	*X*	0.8340	1.2846	3.6198
	Y	1.1541	1.6235	6.0077

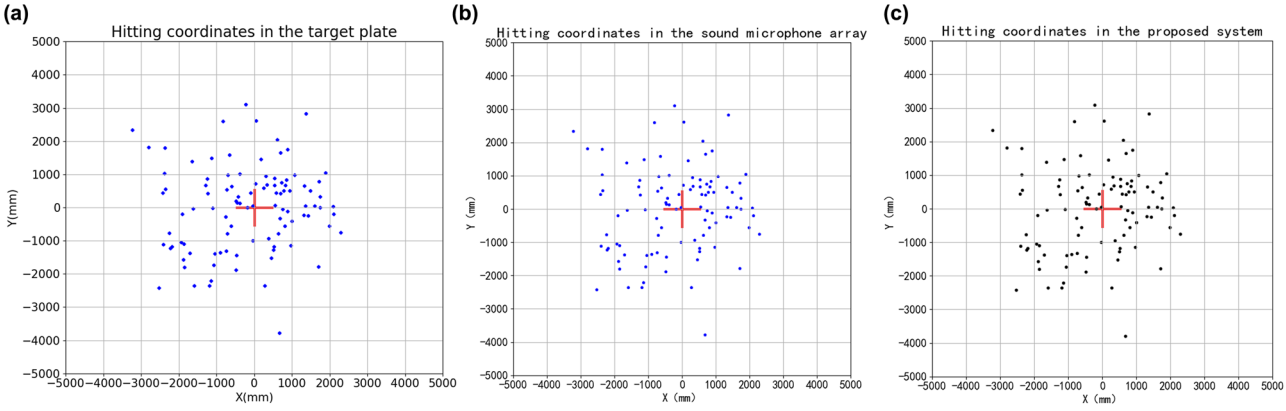

Figure 14: Schematic diagram of the first set of measurement results of bullet holes through the three system: (a) the wooden target based on image processing, (b) the sound microphone array, and (c) the proposed system.

indoor temperature of the shooting gallery was still at 20 ± 2°C. Similar to the first experiment, under the condition of every head shape, we fired 100 projectiles and then recorded their coordinate values.

In Tables 2, 5, and 6, the main performance judgments (*i.e.*, mean value, standard deviation, and maximum deviation) of the two systems under conditions of the conical angles of 45°, 90°, and 120°, are given, respectively. From the above tables, the measurement performance (especially, their standard deviations) of the two systems basically holds steady under the conditions of three conical angles. Obviously, the conical angle of the projectile head does not almost affect the measurement performance of the two systems. Therefore, the improved measurement system has wide adaptability of projectiles with different conical angle.

In fact, the two measurement systems are both based on the similar principle. That is, they use acoustics sensor array or light-curtain sensor to measure several TOA parameters, and then the hitting coordinates of the supersonic projectile in their detection area can be obtained according to their computation model. However, the acoustics system has dozens of acoustic sensors in order to form a large detection area of 10 m × 10 m. Furthermore, there is also the higher requirement for installation accuracy of the acoustic sensors. For the proposed measurement system, we only adopt a light-curtain sensor and three pairs of laser transmitters and receivers. The large detection area (*i.e.*, light curtain) with 10 m × 10 m can be formed; most importantly, its measurement accuracy is also close to that of the acoustics system and it can also up to mm-level.

5 Conclusion

In this study, we investigated an improved measurement method based on light-curtain sensor to effectively obtain the hitting coordinates of supersonic projectile in a large detection area. For this study, it contains the following contributions as below. First, the speed properties of the shock wave in the light curtain based on several key factors (*i.e.*, flight speed of the projectile, its attitude, shape, and the temperature in the testing environment) are obtained after detailed analysis. Second, we developed a design scheme of the improved measurement system. Specially, the main measurement device and the calibration device of the shock speed are two key parts of the system. In fact, the former is wide-angled light-curtain sensor to effectively detect the measured projectile and its shock wave, and the latter can measure real-time speed of the shock wave in the light curtain using three parallel laser beams. Third, according to related geometric principles, some calculation models are, respectively, built to obtain the hitting coordinates of the measured projectile in the light curtain. Finally, we perform the live ammunition experiments under the conditions of two main factors, and they demonstrate that the measurement error of the improved system is always less than 5 mm, and its measurement performance is closer to that of the system based on acoustic sensor arrays. Besides the larger detection area, the improved measurement system also has many merits, including fewer sensors, lower cost, simpler and easier installation, and so on. In future research, we will focus on several problems, including the measurement of flight attitude of the supersonic projectile and multi-target detection. If the above problems are all solved, the measurement performance of the system will be further improved.

Funding information: The authors would like to acknowledge the Natural Science Foundation of Shaanxi Province of China (Grant No. 2019JM-601) and in part by the Scientific Research Programming Project of Shaanxi Provincial Education Department (Grant No. 20JK0692) and the Foundation of Xi'an Key Laboratory of Intelligence (No. 2019220514SYS020CG042).

Author contributions: All authors have accepted responsibility for the entire content of this manuscript and approved its submission.

Conflict of interest: The authors state no conflict of interest.

References

[1] Decker R, Duca M, Spickert FS. Measurement of bullet impact conditions using automated in-flight photography system. Def Technol. 2017;13(4):288–94. doi: 10.1016/j.dt.2017.04.004.

[2] Lin YC, Miaou SG, Lin YC, Chen SL. An automatic scoring system for air pistol shooting competition based on image recognition of target sheets. ICCE-TW 2015. Proceedings of 2015 IEEE International Conference on Consumer Electronics - Taiwan; 2015 June 6–8. Taipei, China. New York: IEEE; 2015. p. 140–1.

[3] Tian H, Jiao MX, Ni JP. Measurement model and algorithm for measuring flight parameter of parabolic trajectory by six-light-screen array. Optik. 2015;126(24):5877–80. doi: 10.1016/j.ijleo.2015.08.264.

[4] Li H, Ni JP, Yang XD, Wu ZC. Analysis of the structure and properties of triangular composite light-screen targets. Open Phys. 2021;19(1):583–9. doi: 10.1016/j.ijleo.2015.08.264.

[5] Li HS, Zhang XQ, Zhang XW, Guo QM. A line laser detection screen design and projectile echo power calculation in detection screen area. Def Technol. 2021;17(6):1135–42, doi: 10.1016/j.dt.2021.06.007.

[6] Zhang XQ, Li HS, Zhang SS. Design and analysis of laser photoelectric detection sensor. Microw Opt Technol Lett. 2021;63(12):3092–9. doi: 10.1002/mop.33011.

[7] Zhang XQ, Li HS, Gao JC. Temporal and spatial domain detection model and method of infrared photoelectric detection target. Appl Opt. 2021;60(24):7437–45. doi: 10.1364/AO.427671.

[8] Yang MJ, Li ZF, Zhu YJ, Zhang EL, Wang J, Shi XF, et al. Shock Waves and Shock Interactions in Hypersonic Flow. Beijing: Nation Defense Industry Press; 2019.

[9] Kam WL. Curvilinear trajectory estimation of a supersonic bullet using ballistic shock wave arrivals at asynchronous acoustic sensor nodes. J Acoust Soc Am. 2017;141(6):4543–55. doi: 10.1121/1.4985442.

[10] Zhang XW, Li HS. Calculation model of projectile explosion position by using acousto-optic combination mechanism. IEEE Access. 2021;9:126058–64. doi: 10.1109/ACCESS.2021.3109918.

[11] Tian H, Yuan Y, Chen D. Improvement of the detection sensitivity uniformity of an indoor light screen array measurement system with large field of view angle using multi-lens splicing. Optik. 2018;181:971–7. doi: 10.1016/j.ijleo.2018.12.150.

[12] Tian H, Yuan Y. Analysis and amendment on the sensitivity of large target area light screen. Infrared Laser Eng. 2018;47(6):108–13. doi: 10.3788/IRLA201847.0617004.

[13] Buckner D, Esperance DL. Digital synchro ballistic schlieren camera for high-speed photography of bullets and rocket sleds. Opt Eng. 2013;52(8):083105-1-8. doi: 10.1117/1.OE.52.8.083105.

[14] Ni JP, Tian H. A study on method of acquiring moment of which a projectile going through a light screen. Opt Tech. 2008;32(1):141–4.

[15] Dong H, Ni JP, Wang TL. Research of the information detect acquire method which the projectile flying the target based on sky screen target. Nucl Electron Detect Technol. 2008;29(4):844–8. doi: 10.1007/978-0-387-74660-9_12.

[16] Tian H, Ni JP, Jiao MX. Moment acquisition algorithm of a projectile passing through a trapezoidal screen. Acta Photonica Sin. 2014;43(12):114–8. doi: 10.3788/gzxb20144312.1212001.
[17] Chen D, Ni JP. Calibration and equalization for the measurement channels of a photoelectric testing system with intersecting detection areas. IEEE Access. 2021;9:17520–9. doi: 10.1109/ACCESS.2021.3054389.
[18] Li HS, Lei ZY, Wang ZM, Gao JC. Research on objection information extraction arithmetic in photo-electric detection target based on wavelet analysis method. Prz Elektrotechniczn. 2012;88(9):157–61.
[19] Li HS, Lei ZY. Time calculation method based on wavelet analysis in vertical target measurement system. Infrared Laser Eng. 2011;40(9):1774–8. doi: 10.3969/j.issn.1007-2276.2011.09.036.
[20] Zhang YP, Ma YJ. Test Methods of Cartridge–Part 18: Firing Accuracy and Dispersion Test, China Military Standard GJB 3196.18A-2005. Beijing: China Standard Press; 2006.
[21] Chen R, Chen D, Ji BW, Ni JP. Inversion method of the key structure parameters of light screen array measurement system using genetic algorithm. Optik. 2020;206:164064. doi: 10.1016/j.ijleo.2019.164064.